

Improved Global Irradiance Decomposition by Sky Condition Classification from Measured Spectral Clearness Indices

Viktar Tatsiankou
School of Electrical Engineering
and Computer Science
University of Ottawa
Ottawa, Canada
viktar.tatsiankou@gmail.com

Dr. Karin Hinzer
School of Electrical Engineering
and Computer Science
University of Ottawa
Ottawa, Canada
khinzer@uottawa.ca

Dr. Henry Schriemer
School of Electrical Engineering
and Computer Science
University of Ottawa
Ottawa, Canada
hschriemer@uottawa.ca

Dr. Richard Beal
Spectrafy Inc.
Ottawa, Canada
richard.beal@spectrafy.com

Abstract—This manuscript describes a decomposition algorithm for deriving the broadband direct normal (DNI) and diffuse horizontal (DHI) irradiances from one-minute spectral global horizontal irradiance measurements performed by the SolarSIM-G. The algorithm was calibrated and validated at four stations across Canada (Ottawa, Varennes, Egbert, and Devon) and at one station in China (Xianghe), which cumulatively represent a seven-year data set. For the DNI estimation, the root mean square error (RMSE) ranged from 26 W/m² to 48 W/m², while the largest mean bias error (MBE) was 4 W/m². For the DHI estimation, the RMSE ranged from 14 W/m² to 27 W/m², while the largest MBE was 3 W/m². In addition, the integrated DNI and DHI errors for each station were less than 1% and 2%, respectively. The described method is an alternative to other measurement techniques for obtaining all three irradiance components.

Keywords—Global horizontal irradiance, direct normal irradiance, diffuse horizontal irradiance, irradiance decomposition algorithm, SolarSIM-G, spectral clearness index, GHI, DNI, DHI

I. INTRODUCTION

Sunlight at the earth’s surface is typically represented by global horizontal, direct normal, and diffuse horizontal irradiances, known as GHI, DNI, and DHI, respectively. Knowledge of these quantities is essential for many applications, such as climate research, solar resource assessment, photovoltaic system monitoring, and many more [1]. Of the three, GHI measurements are by far the most common, mainly because they only require a relatively inexpensive, low maintenance pyranometer statically mounted on a flat surface. In contrast, to obtain measurements of DNI and DHI one requires a pyrhelimeter and a pyranometer (with a shadow ball assembly), respectively, both mounted on a solar tracker. The measurement methods described in [2] are the most accurate way to obtain all three sunshine components. For more cost-sensitive applications, one can use “tracker-less” options to derive the GHI, DNI and DHI with a single instrument, such as a rotating shadowband radiometer or a shadow-mask pyranometer but the resultant measurements have a higher uncertainty than the aforementioned methods [3]. Another convenient option is to solely measure the GHI and then use one of many available irradiance decomposition algorithms to derive

the DNI and/or DHI, such as Erbs, Skartveit, Reindl, DirInt, DISC, and others. These models vary in complexity, but generally have a relatively high uncertainty, with the root mean square errors for DNI retrieval of ~85 W/m² at hourly resolution [4].

Most decomposition algorithms are based on a clearness index, which is a unitless measure of the atmosphere’s clearness, derived from the product of the local GHI and the airmass divided by the extraterrestrial irradiance [5]. Some models have improved the decomposition results by also including the atmospheric turbidity and total column water vapor (i.e. the precipitable water vapor) in their calculations [6,7]. The additional insight from local atmospheric parameters translates to improved model performance.

A comprehensive way to assess the atmospheric conditions is to use local spectral irradiance data, which historically has been very difficult to obtain, as it requires several co-located field spectroradiometers. With the advent of a spectral pyranometer – the SolarSIM-G – it is now possible to obtain full-range spectral and broadband GHI data from a single, compact, low power instrument with no moving parts [8]. In this manuscript we use one-minute spectral measurements made by the SolarSIM-G to derive spectral clearness indices at several wavelengths. We then use these predictors in our decomposition algorithm. We apply data from five test stations to calibrate our algorithm, then validate it by comparing the derived DNI and DHI data at each station against the corresponding measurements from co-located reference instruments. The methodology and the summary of results are presented here.

II. SPECTRAL PYRANOMETER

The SolarSIM-G is a unique instrument that combines a multi-filter radiometer with an advanced radiative transfer model to derive in real-time full-range spectral and broadband global irradiances under all sky conditions. The instrument’s mechanical and optical design have been described elsewhere [8]. In brief, the SolarSIM-G measures the global spectral irradiance using hard-coated narrow bandpass filters paired with seven silicone and two indium gallium arsenide calibrated detectors. The center wavelengths are shown in Table I, along

with the atmospheric parameters or conditions targeted. The instrument also senses the ambient temperature, humidity and atmospheric pressure. The irradiance and environmental measurements are fed into our radiative transfer model to derive the spectral and broadband GHI in the 280-4000 nm range. The spectral reconstruction algorithm is as follows:

1. Calibrate the instrument:
 - a. Determine the temperature coefficients for each channel, similar to [9];
 - b. Optimize the cosine response of the instrument to comply with class A pyranometer requirements from ISO9060:2018 standard;
 - c. Perform on-sun calibration against a reference SolarSIM-G or a reference spectroradiometer [8].
2. Acquire currents from the nine optical channels, the ambient temperature and atmospheric pressure, and the internal temperature of the device.
3. Use our radiative transfer model to derive the spectral global irradiance in the 280-4000 nm range, based on [10]:
 - a. Compute the zenith angle and the sun-earth distance using a solar position algorithm;
 - b. Apply the sun earth-distance correction on the extraterrestrial solar spectrum;
 - c. Calculate Rayleigh scattering and the transmittances from various atmospheric gases (CO₂, CH₄, O₂, NO₂);
 - d. Determine the spectral AOD and its transmittance from all channels except the ozone channel at 610 nm and the water vapor channel at 940 nm, similar to [10], but now with three extra channels;
 - e. Compute the total column ozone and its spectral transmittance from the 610 nm channel;
 - f. Calculate the precipitable water vapor content and its spectral transmittance from the 940 nm channel;
 - g. Determine the spectral irradiance by applying the derived transmittance functions from steps c-f to the extraterrestrial solar spectrum;
 - h. Calculate the cloud transmittance based on the irradiance at channels 8 and 9 and apply a spectral cloud correction to the spectrum from step “g” in the 1000 to 4000 nm range;
 - i. Calculate the diffuse irradiance correction based on the irradiance at channel 1 and adjust the spectrum from step “h” in the 280 to 360 nm range;
 - j. Integrate the spectral irradiance obtained in step “i” to obtain the GHI.

The correction functions in steps “h” and “i” extend the radiative transfer model described in [10] and are proprietary.

TABLE I. LIST OF SOLARSIM-G CHANNELS

Optical channel	Center wavelength (nm)	Resolves
1	< 420 ^a	Aerosols, diffuse
2	420	Aerosols, diffuse
3	500	Aerosols, diffuse
4	610	Ozone
5	675	Aerosols, diffuse
6	880	Aerosols, diffuse
7	940	Water vapor
8	> 1000 ^a	Aerosols, clouds
9	> 1000 ^a	Aerosols, clouds

^a: proprietary

III. DATA SET

Spectral and broadband irradiance data are obtained from five stations across a range of environments, as summarized in Table II. Four stations are a part of the Canadian Spectral Irradiance Network operated by Spectrafy [11], while the fifth is operated by the Institute of Atmospheric Physics in the People’s Republic of China. Each station is equipped with the SolarSIM-D2 and the SolarSIM-G, with raw data acquired at one-minute resolution by a datalogger, and subsequently sent to a central server for processing and storage. The SolarSIM-D2 provides the spectral and broadband DNI in the 280-4000 nm range, spectral aerosol optical depth in the 280-4000 nm range, the total column ozone, and the precipitable water vapor [9,10]; the SolarSIM-G delivers the spectral and broadband GHI in the 280-4000nm range. By combining the measurements from both instruments, we have computed the spectral and broadband DHI in the 280-4000 nm range.

The data sets from each location end by 1 December 2019 and vary in length from 9 to 24 months, in aggregate the equivalent of almost seven station-years. The data sets were carefully screened and validated. Data for solar elevation angles less than 10° were excluded to minimize horizon perturbations, and to avoid shadowing. Data taken during periods of snow, rain, or maintenance were likewise excluded. Three stations – Egbert, Ottawa, and Varennes – operate under similar atmospheric conditions. Their mean AODs at 500 nm (AOD₅₀₀) are shown in Table II as near or at 0.1. The other two stations show greater diversity in atmospheric conditions. Devon station has slightly heavier AOD₅₀₀ loading at 0.14, while the Xianghe station in China has a mean AOD₅₀₀ of 0.48. The combined data set represents a diverse range of environmental conditions that is representative of many locations around the world.

IV. GLOBAL IRRADIANCE DECOMPOSITION

DNI and DHI data may be extracted from the SolarSIM-G’s GHI data. The algorithm for its extraction is given below, followed by a more comprehensive discussion of the spectral clearness index, its application as a predictor of sky conditions,

TABLE II. LIST OF MEASUREMENT STATIONS

Station	Latitude	Longitude	Altitude	AOD ₅₀₀	Range
Devon	53.4°	113.7°	800 m	0.14	9 months
Egbert	44.2°	79.8°	98 m	0.10	21 months
Ottawa	45.4°	75.7°	70 m	0.11	23 months
Varennes	45.6°	73.4°	60 m	0.11	21 months
Xianghe	39.8°	-117.0°	36 m	0.48	9 months

and subsequent employment in the computation of the DNI and the DHI.

A. Decomposition algorithm

The decomposition algorithm is as follows:

1. Acquire spectral and broadband GHI data from the SolarSIM-G;
2. Compute the “clear-sky” spectral GHI from (1);
3. Calculate spectral clearness indices for central wavelengths of all SolarSIM-G’s channels using (2);
4. Determine the sky condition as per Table III;
5. Compute the modelled DNI and DHI from (3) and (4), respectively.

B. Spectral clearness index

We start by defining the “clear-sky” spectral global horizontal irradiance as:

$$S_{\text{GHI,clr}}(\lambda) = S_{\text{DNI,clr}}(\lambda) \cdot m^{-1} + S_{\text{DHI,clr}}(\lambda) \quad (1)$$

where $S_{\text{DNI,clr}}(\lambda)$ and $S_{\text{DHI,clr}}(\lambda)$ are the modelled “clear-sky” spectral DNI and spectral DHI, respectively, in the 280-4000 nm range, and m is the optical air mass. The DNI is obtained through a parameterized direct beam transmittance model, similar to our previous work [10], except the aerosol transmittance is generated by fixing the AOD at 500 nm to 0.05 with its spectral dependence defined by two Ångström exponents, 0.98 and 1.22 for wavelengths before and after 500 nm, respectively. The spectral ozone and water vapor transmittance functions are generated from the total column ozone and precipitable water vapor content obtained by the SolarSIM-G measurements. Finally, the modelled “clear-sky” spectral DHI in the 280-4000 nm is based on [12]. As a more comprehensive measure of the atmosphere’s clearness, we may then define

$$\kappa(\lambda) = \frac{S_{\text{GHI}}(\lambda)}{S_{\text{GHI,clr}}(\lambda)} \quad (2)$$

as a spectral clearness index, where $S_{\text{GHI}}(\lambda)$ is the measured spectral GHI as derived by the SolarSIM-G, and $S_{\text{GHI,clr}}(\lambda)$ is the modelled “clear-sky” spectral GHI, computed from (1).

C. Classification of sky conditions

The crucial insight leveraged in our decomposition algorithm is the realization that similar atmospheric conditions correlate with sky conditions. The classification is presented in Table III. We

categorize sky conditions into seven classes based on the values of the spectral clearness indices $\kappa(\lambda_1)$ and $\kappa(\lambda_9)$, using optical channels 1 and 9 of the SolarSIM-G, respectively. These two channels are chosen because the spectral clearness indices at these wavelengths shows the strongest sensitivity to sky conditions. Channel 1 was chosen because it is the most sensitive to small changes in the diffuse irradiance, while channel 9 was chosen because it is the least sensitive to the clear-sky diffuse irradiance and to the aerosol absorption of the direct beam. As a result, channel 9 is the most sensitive channel to cloud absorption and scattering, and therefore is a good estimator of the clouds’ optical depth that obscure the sun.

Sky clarity is quantified by index ranges, as shown in Table III. Based on the AOD₅₀₀ data from all stations, we found that values for $\kappa(\lambda_9)$ of 0.75 and above correlate with an unobstructed sun disk for over 95% of the data. When the sky is free of clouds, the values of $\kappa(\lambda_1)$ can be used to further characterize the sky as either “very clear”, “clear”, or “hazy”. When the sky is cloudy, but the sun disk is not obscured, the GHI in some cases can exceed the solar constant. This is the special case of lensing, where $\kappa(\lambda_9)$ is found to exceed 1.05. Values of $\kappa(\lambda_9)$ below 0.75 correlate with a sun obstructed by the clouds for over 90% of the data, as determined by the SolarSIM-D2’s AOD₅₀₀ measurements at each station. Decreasing values of $\kappa(\lambda_9)$ correlate well with cloud optical depth, allowing “thin” clouds, “thick” clouds, and completely overcast conditions to be identified by their $\kappa(\lambda_9)$ ranges.

D. Computation of DNI and DHI

For a specific sky condition x , the decomposition of the modelled DNI may be parameterized as

$$I_{\text{DNI,mod}} = \alpha_{1,x} \cdot I_{\text{GHI}} \cdot m + \alpha_{2,x} \cdot I_{\text{DNI,clr}} + \sum_{i=1, i \neq 7}^9 \beta_{i,x} \cdot \kappa(\lambda_i) \quad (3)$$

where I_{GHI} is the measured broadband GHI; $I_{\text{DNI,clr}}$ is the integral of the modeled “clear-sky” spectral DNI, $S_{\text{DNI,clr}}(\lambda)$, in the 280-4000 nm range; $\alpha_{1,x}$ and $\alpha_{2,x}$, are unitless coefficients for the broadband predictors, I_{GHI} and $I_{\text{DNI,clr}}$, respectively; $\beta_{i,x}$ is a set of eight coefficients for spectral clearness indices at the center wavelengths of all SolarSIM-G’s optical channels, except for the water vapor channel, i.e. channel 7. This channel is

TABLE III. CLASSIFICATION OF SKY CONDITIONS BASED ON CLEARNESS INDICES AT SOLARSIM-G’S CHANNELS 1 AND 9

Sky condition	x	$\kappa(\lambda_1)$		$\kappa(\lambda_9)$	
		Min	Max	Min	Max
Very clear	1	1.0	-	0.75	1.05
Clear	2	0.8	1.0	0.75	1.05
Hazy	3	-	0.8	0.75	1.05
Thin clouds	4	-	-	0.5	0.75
Thick clouds	5	-	-	0.25	0.5
Overcast	6	-	-	-	0.25
Lensing	7	-	-	1.05	-

TABLE IV. THE DERIVED COEFFICIENTS FOR THE DNI ESTIMATION FOR A SPECIFIC SKY CONDITION

Sky condition	x	Coefficients									
		$\alpha_{1,x}$	$\alpha_{2,x}$	$\beta_{1,x}$	$\beta_{2,x}$	$\beta_{3,x}$	$\beta_{4,x}$	$\beta_{5,x}$	$\beta_{6,x}$	$\beta_{8,x}$	$\beta_{9,x}$
Very clear	1	1.104	-0.357	-812.1	557.9	1345.6	-2828.2	3796.9	-3898.7	-179.4	2070.9
Clear	2	0.447	-0.368	-1042.6	1362.2	3039.6	-5446.7	5138.8	-2897.2	-1228.3	1949.9
Hazy	3	0.707	-0.806	-174.2	779.4	1672.6	-6004.2	8345.3	-4876.0	360.0	888.5
Cloudy	4	0.850	-0.647	-287.1	-123.7	1766.2	-4047.3	4234.6	-2205.3	698.5	387.0
Very cloudy	5	0.086	-0.097	242.0	-490.8	660.8	-970.3	741.7	-404.2	436.7	-51.0
Overcast	6	-	-	-	-	-	-	-	-	-	-
Lensing	7	0.475	0.501	-1473.6	1453.1	1682.9	1303.6	-2802.0	262.0	-1151.1	629.1

excluded because variation in the total column water vapor is already captured within the I_{GHI} and $I_{\text{DNI,clr}}$ variables. The α and β coefficients for each sky condition x were determined using a multivariate ordinary least squares linear regression algorithm that minimized the difference between the modelled DNI and the measured DNI time series from *all* stations at the same time. These coefficients are presented in Table IV for all sky conditions, except when it is overcast, in which case the modeled DNI is set to zero.

The DHI can be computed from the GHI and the DNI as

$$I_{\text{DHI}} = I_{\text{GHI}} - I_{\text{DNI}} \cdot m^{-1}. \quad (4)$$

V. RESULTS AND DISCUSSION

We assess the performance of our decomposition algorithm by comparing modeled DNI and DHI time series at each station against their corresponding references values. The reference DNI was determined from the SolarSIM-D2 measurements, while the reference DHI was computed from (4) using the reference DNI and GHI, as derived by the SolarSIM-D2 and the SolarSIM-G, respectively, at each station. We assume that

any differences between reference instruments and derived DNI and DHI values are dominated by the limitations of the decomposition algorithm. Therefore, reference instrument measurement uncertainties were not included in the comparative analysis (i.e. reference DNI and DHI data were assumed to be true).

We evaluate the decomposition algorithm by calculating various statistical estimators from the difference between the modeled and reference DNI and DHI time series for each station. Fig. 1a and Fig. 1b show boxplot diagrams of the error distributions of the modeled DNI and modeled DHI, respectively, as compared to their corresponding reference measurements at each station. The Interquartile Range (IQR) is defined as the difference between the 75th and 25th percentiles of the data set, while the extended range represents the errors within the 5th and 95th percentiles, which corresponds to approximately $\pm 1.8\sigma$ or 90% coverage, if assuming a normal distribution. The mean bias error (MBE) assesses the average bias in the prediction, while the root mean square error (RMSE) is the standard deviation of the prediction error.

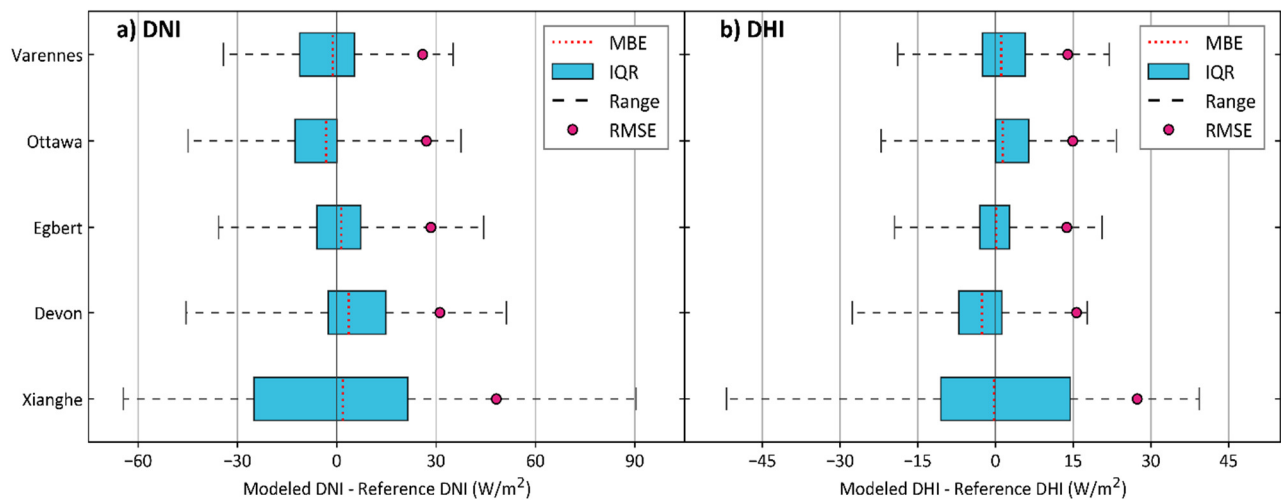


Fig. 1. Boxplot diagram of the error distributions between the a) modeled direct normal irradiance (DNI), b) modeled diffuse horizontal irradiance (DHI) from our decomposition algorithm and the corresponding DNI, DHI measurements made by the reference instruments. The plots show the mean bias error (MBE), interquartile range (IQR), defined as the values within the 25th and 75th percentiles, the extended error range, defined as the values within 5th and 95th percentiles, and the root mean square error (RMSE) for each station.

As can be seen from Fig. 1a, the extended error ranges for DNI retrieval are very similar for Ottawa, Varennes and Egbert stations, about $\pm 40 \text{ W/m}^2$, while the MBE is around -1 W/m^2 and the RMSE is about 27 W/m^2 . This is expected since these stations are relatively close to each other and are subjected to similar environmental conditions. For Devon station, which has a slightly higher mean AOD_{500} than the aforementioned stations, the extended error range is a bit wider at about $\pm 48 \text{ W/m}^2$, while the RMSE is very similar. For Xianghe station, which experiences large variations in aerosol conditions due to changes in pollution, the extended error range for the DNI is relatively high, ranging from -64 W/m^2 to $+90 \text{ W/m}^2$, while the RMSE is 48 W/m^2 . This is due to numerous periods at Xianghe when the reduction of GHI irradiance due to aerosol absorption of the direct beam is partially compensated for by the gain in the GHI from the diffuse irradiance due to aerosol scattering. In such cases our algorithm has a difficult time differentiating between the “clear”, “hazy”, and “thin clouds” sky conditions, which leads to increased uncertainty for the DNI retrieval. Nonetheless, the MBE for the DNI estimation for all stations is less than 4 W/m^2 .

The modeled DHI propagates the errors from the modeled DNI, as per (4). The extended error range for Varennes, Ottawa, Egbert stations is about $\pm 21 \text{ W/m}^2$, while the MBE and the RMSE are at $+1 \text{ W/m}^2$ and 14 W/m^2 , respectively. For Devon station the MBE was approximately -3 W/m^2 with the extended error range stretching from -28 W/m^2 to 17 W/m^2 , while the RMSE was 15 W/m^2 . Similar to the DNI retrieval, the Xianghe station saw the highest error spread with the extended error range varying from -52 W/m^2 to 39 W/m^2 , with negligible MBE and the RMSE of 27 W/m^2 .

We also computed the integrated energy per unit surface area errors for the entire DNI and DHI datasets at each station and compared them against the corresponding reference values. The DNI and DHI integrated energy errors are less than 1% and 2%, respectively, at each station. This is an important result as it suggests that even in high aerosol environments such as Xianghe, the decomposition algorithm can accurately provide the estimate of the DNI and DHI solar resource potential.

VI. CONCLUSION

We have described a decomposition algorithm that uses spectral GHI measurements made by the SolarSIM-G to derive broadband DNI and DHI. We have proposed a more quantitative approach to the classification of atmospheric conditions via spectral clearness indices, which are also used as predictors to estimate DNI, and consequently to compute DHI. We used one-minute resolution measurement data from five stations (equivalent to seven station-years) to calibrate

and validate our decomposition algorithm. For the DNI estimation, the RMSE ranged from 26 W/m^2 to 48 W/m^2 , while for the DHI estimation - from 14 W/m^2 to 27 W/m^2 . The largest absolute MBE for both cases was less than 4 W/m^2 . In addition, the integrated DNI and DHI errors for each station were less than 1% and 2%, respectively.

These results show that the described decomposition algorithm has a factor of 2 to 3 improvement in the RMSE over existing, state-of-the-art decomposition algorithms, even with a one-minute resolution data set. Furthermore, based on [3], the proposed method is a comparable alternative to other tracker-less methods for obtaining all three components of sunlight, such as rotating shadowband radiometer and shadow-mask pyranometer. Undoubtedly, the SolarSIM-G based decomposition algorithm can be further improved as more data becomes available from the existing measurement stations and future installations worldwide.

REFERENCES

- [1] C. A. Gueymard and D. R. Myers, “Evaluation of conventional and high-performance routine solar radiation measurements for improved solar resource, climatological trends, and radiative modeling,” *Solar Energy*, vol. 83, no. 2, pp. 171–185, 2009.
- [2] A. Ohmura, et al., “Baseline Surface Radiation Network (BSRN/WCRP): New precision radiometry for climate research,” *Bulletin of the American Meteorological Society*, vol. 79, pp. 2115–2136, 1998.
- [3] L. Vuilleumier, et al., “Performance evaluation of radiation sensors for the solar energy sector,” *Meteorologische Zeitschrift*, vol. 26, pp. 485–505, 2017.
- [4] P. Ineichen, “Comparison and validation of three global-to-beam irradiance models against ground measurements,” *Solar Energy*, vol. 82, pp. 501–512, 2008.
- [5] D. G. Erbs, S. A. Klein, and J.A. Duffie, “Estimation of the diffuse radiation fraction for hourly, daily and monthly-average global radiation,” *Solar Energy*, vol. 28, pp. 293–302, 1982.
- [6] P. Ineichen, et al., “Dynamic global-to-direct irradiance conversion models,” *Ashrae Transaction*, vol. 98, pp. 354–369, 1992.
- [7] R. R. Perez, et al., “A new operational model for satellite-derived irradiances: description and validation,” *Solar Energy*, vol. 73, pp. 307–317, 2002.
- [8] V. Tsiiankou, K. Hinzer, H. Schriemer, and R. Beal, “Efficient, Real-Time Global Spectral and Broadband Irradiance Acquisition,” 7th World Conference on Photovoltaic Energy Conversion, 2018
- [9] V. Tsiiankou, et al., “Extensive validation of solar spectral irradiance meters at the World Radiation Center,” *Solar Energy*, vol. 166, pp. 80–89, 2018.
- [10] V. Tsiiankou, K. Hinzer, H. Schriemer, K. Emery, and R. Beal, “Design principles and field performance of a solar spectral irradiance meter,” *Solar Energy*, vol. 133, pp. 94–102, 2016.
- [11] V. Tsiiankou, K. Hinzer, H. Schriemer, P. McVey-White, and R. Beal, “Deployment and early results from the CanSIM (Canadian Solar Spectral Irradiance Meter) network,” *AIP Conference Proceedings*, vol. 1881, 2017.
- [12] R.E. Bird and C. Riordan, “Simple solar spectral model for direct and diffuse irradiance on horizontal and tilted planes at the earth’s surface for cloudless atmospheres,” *Journal of Climate and Applied Meteorology*, vol. 25, pp. 87–97, 1986.